RSC Advances

PAPER

View Article Online
View Journal | View Issue

Cite this: *RSC Adv.*, 2026, **16**, 3894

Novel diazenyl chalcones with a 2-arylidene hydrazineylidene thiazole moiety: synthesis, anticancer potential, spectroscopic characterisation, and molecular docking studies

Mariem M. El-Samoly,[a] Esmail M. El-Fakharany,*[b] Yousra A. El-Maradny,[b] Abdallah E. Abdallah,[c] F. A. Taher,[a] Nadia T. A. Dawoud *[a] and Doaa R. Lotfy[a]

A series of diazenyl chalcones bearing 2-arylidene-hydrazinylidene thiazole units (**4–6a,b**) were designed, synthesised, and fully characterised by NMR, IR, MS, and UV spectroscopy. The compounds were evaluated for cytotoxicity against normal skin cells and the MDA and HepG2 cancer cell lines. The results reveal that most synthetic chemicals exhibited limited toxicity on normal cells at concentrations of 100 μg mL^{-1} or below. Additionally, all pharmaceuticals, except for compound **4a**, all pharmaceuticals demonstrated antiproliferation activity at quantities below the safety threshold. MDA and HepG2 cells exhibited no significant differences in cytotoxicity; however, compounds **5b** and **6a** showed the highest selectivity indices. The new compounds exhibited excellent affinity for the MMP-2 receptor, with values between −32.67 and −14.98 kcal mol^{-1}. Compounds **6a** and **6b** demonstrated the most advantageous results, with values of −32.67 and −32.27 kcal mol^{-1}, respectively, in comparison to the ligand's value of −33.73 kcal mol^{-1}. Compound **5b** attained a third-place ranking with a score of −29.72 kcal mol^{-1}. Compounds **4a** and **4b** demonstrated relatively lower scores; however, compound **5a** revealed markedly worse performance in comparison to other derivatives. Finally, these findings should be regarded as preliminary, indicating promising biological potential but not confirming any specific mechanism of action.

Received 11th October 2025
Accepted 14th December 2025

DOI: 10.1039/d5ra07769a

rsc.li/rsc-advances

Introduction

Cancer remains a major global health challenge, largely due to the uncontrolled proliferation of abnormal cells. Unlike normal cells, cancer cells bypass regulatory mechanisms governing growth and survival, enabling continuous division, invasion of surrounding tissues, and metastasis to distant organs. These malignant behaviours arise from accumulated genetic mutations and dysregulation of multiple intracellular signalling pathways.[1]

Heterocyclic compounds have played a pivotal role in anticancer drug development. Many clinically used chemotherapeutic agents—such as methotrexate, vinblastine, vincristine, daunorubicin, 5-fluorouracil and doxorubicin—contain heterocyclic scaffolds, reflecting the structural versatility and broad pharmacological potential of these molecules.[2] Among heterocycles, Schiff bases (characterised by an imine >C=N– group) are particularly prominent due to their π-acceptor properties, strong metal-chelating ability and diverse biological activities, including antibacterial, antioxidant and antiproliferative effects.[3–9] Likewise, the 4-thiazolidinone framework represents a privileged scaffold in medicinal chemistry, widely reported for its anti-inflammatory, antibacterial, antidiabetic, antioxidant and anticancer properties.[10–15] In particular, 5-arylidenethiazolidin-4-one derivatives have emerged as promising drug-like candidates.[16–20] Azo-chalcones constitute another notable class, combining the reactive α,β-unsaturated carbonyl system of chalcones with an azo (–N=N–) group, giving rise to photoresponsive molecules with reported antimicrobial, anti-inflammatory and anticancer activities.[21–23]

The design of the present diazenyl chalcone series bearing a 2-arylidene hydrazinylidene thiazole moiety was motivated by the pharmacophoric features of these two bioactive scaffolds. Chalcones are well-established Michael acceptors with anticancer, anti-inflammatory and enzyme–inhibitory activities, primarily attributed to their α,β-unsaturated system. Thiazole-based heterocycles, including thiazolidinones and hydrazinylidene derivatives, exhibit potent cytotoxic and matrix metalloproteinase (MMP) inhibitory effects. Integrating these motifs through a diazenyl linker was expected to (i) enhance molecular

[a]*Chemistry Department, Faculty of Science, Girls, Al-Azhar University, Nasr City, Cairo, Egypt*

[b]*Protein Research Department, Genetic Engineering and Biotechnology Research Institute, City of Scientific Research and Technological Applications (SRTA-City), New Borg AL-Arab, 21934, Alexandria, Egypt. E-mail: esmailelfakharany@yahoo.co.uk*

[c]*Pharmaceutical Medicinal Chemistry & Drug Design Department, Faculty of Pharmacy (Boys), Al-Azhar University, Nasr City, Cairo, 11884, Egypt. E-mail: dawoudnadia@yahoo.com*

conjugation and electronic distribution, (ii) improve binding interactions with MMP-2 *via* additional hydrogen-bonding and π–π stacking sites, and (iii) generate hybrid molecules capable of synergistic anticancer activity. *In silico* docking supported this design, predicting favourable binding energies.

Thus, the synthetic strategy aimed to develop hybrid molecules with enhanced anticancer potential and high affinity toward MMP targets.

Materials and methods

All melting point ranges were taken on a Gallenkamp electric melting point apparatus using the one-end open capillary method and were uncorrected. The IR spectra of the compounds were recorded on the Bruker ALPHA II Fourier Transform Infrared Spectrometer at a wavenumber of (4000–400 cm^{-1}). The ^{1}H and ^{13}C-NMR spectra were recorded on a Bruker AV 300 and Jeol 500 MHz spectrometer operating at 300 and 500 MHz for ^{1}H and 75, 125 MHz for ^{13}C using dimethyl dimethylsulfoxide as solvent and tetramethylsilane (TMS) as an internal reference. Mass spectra (MS) were recorded on the Thermo Scientific GCMS model (ISQ LT) using Thermo X-Calibur software. Elemental analyses were performed on the elemental analyzer (CHNS) set: Flash 2000 Thermo Scientific. The reactions were followed up, and the purity of products was carried out on silica gel G60F (Merck) plates that were precoated to a thickness of 0.2 mm, visualizing the spots under ultraviolet light and or dichloromethane/PE (1 : 3), and/or DCM/drop of ethanol as mobile phases. The PerkinElmer Lambda 35 spectrophotometer was used to deliver the visible spectra for all compounds.

Chemistry and characterization

We confirmed the structures of these newly synthesised compounds using FTIR, ^{1}H-NMR, and ^{13}C-NMR spectroscopy, elemental analysis, and mass spectra.

General procedure for the synthesis of 2-(substituted-benzylidene)-hydrazine-1-carbothioamide derivatives (1a–f). 4-Chlorobenzaldehyde, benzaldehyde, 4-methoxybenzaldehyde, 2-hydroxybenzaldehyde, 4-hydroxybenzaldehyde, and 4-hydroxy-3-methoxybenzaldehyde (0.01 mol) were individually mixed with thiosemicarbazide (0.01 mol) in hot (20 mL). A few drops of catalytic acetic acid were added through constant stirring. The precipitates were formed after refluxing the mixture for 3–6 hours. Reaction progress was monitored *via* thin-layer chromatography (TLC) using dichloromethane/PE (1 : 3). The products were then filtered and washed many times with hot ethanol and water, and then diethyl ether, resulting in a high yield of thiosemicarbazones (**1a–f**).

2-(4-Chlorobenzylidene)hydrazine-1-carbothioamide ***(1a).*** White crystals, yield 85%, m.p. 218–220 °C. FTIR (cm^{-1}): 3430(NH), 3279, 3164(NH_2), 3070(CH)Ar, 2795(CH)Al, 1284(C=S), 1599(C=N), 1522(C=C), 816(C–Cl). ^{1}H-NMR (300 MHz, DMSO-d_6): δ ppm; 11.49 (s, 1H, NH), 8.24 (s, 1H, CH=N), 8.02 (s, 2H, NH_2), 7.78–7.35 (m, 4H, Ar–H). ^{13}C-NMR (75 MHz, DMSO-d_6): δ ppm; 178.0, 141.0, 134.3, 133.0, 128.8(2 × C), 128.7(2 × C). Elemental analysis: calcd: C, 44.97; H, 3.77; Cl, 16.59; N, 19.67; S, 15.00; found: C, 44.64; H, 3.54; Cl, 16.43; N, 19.46; S, 14.65.

2-Benzylidenehydrazine-1-carbothioamide ***(1b).*** Pale yellow crystals, yield 51%, m.p. 157–160 °C. FTIR (cm^{-1}): 3417(NH), 3247, 3143(NH_2), 3024(CH)Ar, 2819(CH)Al, 1289(C=S), 1588(C=N), 1534(C=C). ^{1}H-NMR (500 MHz, DMSO-d_6): δ ppm; 12.02, (s, 1H, NH), 8.39 (s, 1H, CH=N), 7.75–7.52 (m, 4H, Ar–H + NH_2). ^{13}C-NMR (125 MHz, DMSO-d_6): δ ppm; 174.2, 155.0, 135.1, 133.1, 129.2(2 × C), 128.9(2 × C). Elemental analysis: calcd: C, 53.61; H, 5.06; N, 23.44; S, 17.89; found: C, 53.33; H, 5.00; N, 23.32; S, 17.67.

2-(4-Methoxybenzylidene)hydrazine-1-carbothioamide ***(1c).*** Yellow crystals, yield 66%, m.p. 174–176 °C. FTIR (cm^{-1}): 3401(NH), 3285, 3143(NH_2), 2970(CH)Ar, 1241(C=S), 1596(C=N), 1172(C–O). ^{1}H-NMR (300 MHz, DMSO-d_6): δ ppm; 11.29 (s, 1H, NH), 8.07 (s, 1H, CH=N), 8.00 (s, 2H, NH_2), 7.88–6.93 (m, 4H, Ar–H), 3.78 (s, 3H, OCH_3). ^{13}C-NMR (75 MHz, DMSO-d_6): δ ppm; 177.5, 160.6, 142.2, 128. 9(2 × C), 126.7, 114.1(2 × C), 55.2. Elemental analysis: calcd: C, 51.66; H, 5.30; N, 20.08; S, 15.32; found: C, 51.45; H, 5.26; N, 20.01; S, 15.10.

2-(2-Hydroxybenzylidene)hydrazine-1-carbothioamide ***(1d).*** Beige crystals, yield 70%, m.p. 240–242 °C. FTIR (cm^{-1}); 3441(OH), 3314(NH), 3171, 3134(NH_2), 3022(CH)Ar, 2985(CH)Al, 1263(C=S), 1602(C=N), 1535(C=C). ^{1}H-NMR (300 MHz, DMSO-d_6): δ ppm; 11.35 (s, 1H, NH), 9.83 (1H, OH), 8.38 (s, 1H, CH=N), 8.07 (s, 2H, NH_2), 7.89–6.78 (m, 4H, Ar–H). ^{13}C-NMR (75 MHz, DMSO-d_6): δ ppm; 177.5, 156.3, 140.0, 131.2, 126.8, 120.1, 119.3, 116.0. Elemental analysis: calcd: C, 49.22; H, 4.65; N, 21.52; S, 16.42; found: C, 49.02; H, 4.45; N, 21.32; S, 16.22.

2-(4-Hydroxybenzylidene)hydrazine-1-carbothioamide ***(1e).*** Beige crystals, yield 63.5%, m.p. 258–260 °C. FTIR (cm^{-1}); 3467(OH), 3357(NH), 3185, 3119(NH_2), 3030(CH)Ar, 2919 (CH)Al, 1265(C=S), 1582(C=N), 1549(C=C). ^{1}H-NMR (300 MHz, DMSO-d_6): δ ppm; 11.21 (s, 1H, NH), 9.86 (s, 1H, OH), 8.01 (s, 1H, CH=N), 7.79 (s, 2H, NH_2), 7.62–6.77 (m, 4H, Ar–H). ^{13}C-NMR (75 MHz, DMSO-d_6): δ ppm; 177.4, 159.2, 142.8, 129.1(2 × C), 125.1, 115.6(2 × C). Elemental analysis: calcd: C, 49.22; H, 4.65; N, 21.52; S, 16.42; found: C, 49.02; H, 4.43; N, 21.36; S, 16.26.

2-(4-Hydroxy-3-methoxybenzylidene)hydrazine-1-carbothioamide ***(1f).*** White crystals, yield 33%, m.p. 200 °C. FTIR (cm^{-1}); 3529(OH), 3437(NH), 3278, 3154(NH_2), 3037(CH)Ar, 2938(CH)Al, 1278(C=S), 1587(C=N), 1545(C=C). ^{1}H-NMR (300 MHz, DMSO-d_6): δ ppm; 11.21 (s, 1H, NH), 9.43 (s, 1H, OH), 8.06 (s, 1H, CH=N), 7.96–6.76 (m, 6H, Ar–H + NH_2), 3.82 (s, 3H, OCH_3). ^{13}C-NMR (75 MHz, DMSO-d_6): δ ppm; 177.1, 148.6, 147.8, 142.7, 125.3, 122.1, 115.0, 109.0, 55.5. Elemental analysis: calcd: C, 47.99; H, 4.92; N, 18.65; S, 14.23; found: C, 47.76; H, 4.83; N, 18.48; S, 14.11.

General procedure for the synthesis of 2-(4-substituted benzylidene)-hydrazineylidene) thiazolidin-4-one derivatives (2a–d). A solution of (**1a–d**) (0.01 mol) in ethanol was slowly added to a stirring solution of ethylchloroacetate (0.01 mol) in ethanol containing anhydrous sodium acetate (0.05 mol). The reaction mixture was heated under reflux for 10 hours. Reaction

progress was monitored *via* thin-layer chromatography (TLC) using dichloromethane/drop of ethanol. The reaction mixture was subsequently filtered and rinsed with ethanol and hot water. The pure product (**2a–d**) was obtained by recrystallization from a 1 : 1 ethanol–water mixture.

*2(-4-Chlorobenzylidene)hydrazinylidene)thiazolidin-4-one (**2a**).* White crystals, yield 82%, m.p. 310–312 °C. FTIR (cm^{-1}); 3419(NH), 2928(CH)Ar, 2744(CH)Al, 1707(C=O), 1640(C=N), 1540(C=C), 829(C–Cl). ^{1}H-NMR (500 MHz, DMSO-d_6): δ ppm; 12.03 (s, 1H, NH), 8.39 (s, 1H, CH=N), 7.77–7.50 (m, 4H, Ar–H), 3.89 (s, 2H, SCH_2). ^{13}C-NMR (125 MHz, DMSO-d_6): δ ppm; 174.2, 165.8, 155.0, 135.1, 133.1, 129.2(2 × C), 128.9(2 × C), 33.0. Elemental analysis: calcd: C, 47.34; H, 3.18; Cl, 13.97; N, 16.56; S, 12.64; found: C, 47.22; H, 3.05; Cl, 13.76; N, 16.43; S, 12.52.

*2(Benzylidene)hydrazinylidene)thiazolidin-4-one (**2b**).* Yellow crystals, yield 68%, m.p. 260–263 °C. FTIR (cm^{-1}); 3150(NH), 3056(CH)Ar, 2756(CH)Al, 1709(C=O), 1640(C=N), 1588(C=C). ^{1}H-NMR (300 MHz, DMSO-d_6): δ ppm; 11.21 (s, 1H, NH), 8.05 (s, 1H, CH=N), 7.93–6.76 (m, 5H, Ar–H), 3.82 (s, 2H, SCH_2). ^{13}C-NMR (75 MHz, DMSO-d_6): δ ppm; 174.3, 165.5, 156.3, 134.2, 130.7, 128.9(2 × C), 127.7(2 × C), 33.1. Elemental analysis: calcd: C, 54.78; H, 4.14; N, 19.16; S, 14.62; found: C, 54.53; H, 4.08; N, 19.13; S, 14.35.

*2(-4-Methoxybenzylidene)hydrazinylidene)thiazolidin-4-one (**2c**).* Yellow crystals, yield 92%, m.p. 260–263 °C. FTIR (cm^{-1}); 3648(OH), 2971(CH)Ar, 2730(CH)Al, 1716(C=O), 1629(C=N), 1596(C=C). ^{1}H-NMR (300 MHz, DMSO-d_6): δ ppm; 11.88 (1H, s, NH), 8.32 (s, 1H, CH=N), 7.71–7.00 (4H, m, Ar–H), 3.87 (s, 2H, SCH_2), 3.80 (s, 3H, OCH_3). ^{13}C-NMR (75 MHz, DMSO-d_6): δ ppm; 174.2, 161.3, 155.9, 144.8, 129.3(2 × C), 126.8, 114.3(2 × C), 55.3, 33.0. Elemental analysis: calcd: C, 53.00; H, 4.45; N, 16.86; S, 12.86; found: C, 52.83; H, 4.40; N, 16.64; S, 12.67.

*2(-2-Hydroxybenzylidene)hydrazinylidene)thiazolidin-4-one (**2d**).* Simone crystals, yield 90%, m.p. 300–303 °C. FTIR (cm^{-1}); 3419(OH), 3041, 2929(CH)Ar, 2856(CH)Al, 1703(C=O), 1596(C=N), 1493(C=C). ^{1}H-NMR (300 MHz, DMSO-d_6): δ ppm; 12.06 (s, 1H, NH), 10.86 (s, 1H, OH), 8.63 (s, 1H, CH=N), 7.58–6.91 (m, 4H, Ar–H), 3.96 (s, 2H, CH_2). ^{13}C-NMR (75 MHz, DMSO-d_6): δ ppm; 173.9, 164.6, 158.0, 157.8, 132.2, 130.6, 119.5, 118.4, 116.3, 33.4. Elemental analysis: calcd: C, 53.00; H, 4.45; N, 16.86; S, 12.86. found: C, 5 2.70; H, 4.20; N, 16.66; S, 12.71.

General procedure for the synthesis of 2-(4-substituted benzylidene)hydrazinylidene)-5-(2-hydroxybenzylidene) thiazolidin-4-one (3a–d). While stirring, a solution of (**2a–d**) (0.01 mol) in ethanol with 10% NaOH was slowly mixed with a solution of salicylaldehyde (0.01 mol) in ethanol. The reaction mixture was heated under reflux for 6 to 8 hours. Reaction progress was monitored *via* thin-layer chromatography (TLC) using dichloromethane/drop of ethanol. The mixture cooled to room temperature, neutralized with ice and HCl, and the precipitates were formed, filtered, and washed with water and ether. The purified products (**3a–d**) were obtained from recrystallization with a 1 : 1 mixture of ethanol and water.

*2-(4-Chlorobenzylidene)hydrazinylidene)-5-(2-hydroxybenzylidene)thiazolidin-4-one (**3a**).* Yellow crystals, yield 23%, m.p. 297–300 °C. FTIR (cm^{-1}); 3744(OH), 3039(CH)Ar, 2753(CH)Al, 1693(C=O), 1641(C=N), 1592(C=C), 821(C–Cl). ^{1}HNMR (300 MHz, DMSO-d_6): δ ppm; 11.84 (s, H, NH), 10.25 (s, 1H, OH), 8.51 (s, 1H, CH=N), 7.89 (s, 1H, CH=C), 7.84–6.96 (m, 8H, Ar–H). ^{13}C-NMR (75 MHz, DMSO-d_6): δ ppm; 168.1, 160.8, 157.1, 156.2, 135.5, 132.9, 131.6, 129.6(2 × C), 129.1(2 × C), 128.4, 124.3, 121.6, 120.7, 119.7, 116.1. MS (*m*/*z*, %): 357 (M^+, 30). Elemental analysis: calcd: C, 57.07; H, 3.38; Cl, 9.91; N, 11.74; S, 8.96; found: C, 57.00; H, 3.20; Cl, 9.65; N, 11.54; S, 8.75.

*2-(Benzylidene)hydrazinylidene)-5-(2-hydroxybenzylidene) thiazolidin-4-one (**3b**).* Yellow crystals, yield 61%, m.p. 298–300 °C. FTIR (cm^{-1}); 3249(OH), 3058(CH)Ar, 2764(CH)Al, 1676(C=O), 1641(C=N), 1590(C=C), 465(OH, Enol). ^{1}H-NMR (300 MHz, DMSO-d_6): δ ppm; 12.47 (s, 1H, NHCO/N=C–OH), 10.68 (s, 1H, OH), 8.51 (s, 1H, CH=N), 7.91 (s, 1H, CH=C), 7.84–6.99 (m, 9H, Ar–H). ^{13}C-NMR (75 MHz, DMSO-d_6): δ ppm; 167.8, 160.0, 157.5, 157.2, 134.0, 131.5, 130.9, 128.9, 128.4, 128.0(2 × C), 124.4, 121.5, 120.7, 119.6, 116.2. MS (*m*/*z*, %): 323 (M^+, 8). Elemental analysis: calcd: C, 63.14; H, 4.05; N, 12.99; S, 9.91; found: C, 63.01; H, 4.00; N, 12.85; S, 9.67.

*5-(2-Hydroxybenzylidene)-2-(4-methoxybenzylidene) hydrazinylidene)thiazolidin-4-one (**3c**).* Yellow crystals, yield 53.19%, m.p. 272–274 °C. FTIR (cm^{-1}); 3400(OH), 3222(NH), 3058(CH)Ar, 2762(CH)Al, 1686(C=O), 1636(C=N), 1598(C=C), 468(OH, Enol). ^{1}H-NMR (300 MHz, DMSO-d_6): δ ppm; 12.38 (s, 1H, NHCO/N=C–OH), 10.49 (s, 1H, OH), 8.43 (s, 1H, CH=N), 7.88 (s, 1H, C=CH), 7.78–6.96 (m, 8H, Ar–H), 3.81 (s, 3H, OCH_3). ^{13}C-NMR (75 MHz, DMSO-d_6): δ ppm; 167.8, 161.5, 158.6, 157.1, 157.1, 131.5, 129.7(2× C), 128.3, 126.6, 124.1, 121.6, 120.7, 119.6, 116.1, 114.4(2 × C), 55.4. MS (*m*/*z*, %): 353 (M^+, 18). Elemental analysis: calcd: C, 61.18; H, 4.28; N, 11.89; S, 9.07; found: C, 61.09; H, 4.15; N, 11.63; S, 9.02.

*5-(2-Hydroxybenzylidene)-2-(2-hydroxybenzylidene) hydrazinylidene)thiazolidin-4-one (**3d**).* Yellow crystals, yield 51%, m.p. 312–314 °C. FTIR (cm^{-1}); 3426(OH), 3154(NH), 2933(CH)Ar, 1677(C=O), 1591(C=N), 1523(C=C). ^{1}H-NMR (300 MHz, DMSO-d_6): δ ppm; 12.53 (s, 1H, NHCO/N=C–OH), 10.68 (s, 1H, OH), 10.46 (s, 1H, OH), 8.72 (s, 1H, CH=N), 7.91 (s, 1H, C=CH), 7.68–6.98 (m, 8H, H–Ar). ^{13}C-NMR (75 MHz, DMSO-d_6): δ ppm; 167.6, 159.0, 158.0, 157.5, 157.1, 132.5, 132.1, 131.8, 129.9, 128.4, 124.9, 120.9, 120.5, 119.7, 118.8, 116.4, 116.1. MS (*m*/*z*, %): 339 (M^+, 23). Elemental analysis: calcd: C, 60.17; H, 3.86; N, 12.38; S, 9.45; found: C, 59.87; H, 3.61; N, 12.18; S, 9.19.

General procedure for the synthesis of 2-(substituted-benzylidene) hydrazinylidene-5-(2-hydroxy-5-(substituted-phenyl diazenyl) benzylidene) thiazolidin-4-one (4–6a,b). A mixture of substituted aniline (*p*-chloro, *p*-methyl) (0.01 mol) in hydrochloric acid (5 mL) and water (5 mL) was heated to 70 °C. The clear solutions were added to an ice-water mixture, and diazotization was carried out at 0–5 °C by adding sodium nitrite (0.05 mol) dissolved in 10 mL of water. The cold diazo solutions were added gradually to compounds (**3a–c**) (0.01 mol) solution in 50 mL of water, which included sodium hydroxide (0.005 mol) and sodium carbonate (0.03 mol). The reaction mixture was vigorously stirred for 30 minutes at 0 °C during the addition process. The precipitated products were collected *via* filtration, washed with 250 mL of water to obtain the pure products (**4–6a,b**).

*2-(4-Chlorobenzylidene)hydrazinylidene)-5-(5-(4-chlorophenyl) diazenyl)-2-hydroxybenzylidene)thiazolidin-4-one (**4a**) [Cl/Cl dye].* Red crystals, yield 78%, m.p. 296–298 °C. FTIR (cm^{-1}); 3833(OH), 3236(NH), 3044(CH)Ar, 2750(CH)Al, 1681(C=O), 1639(C=N), 1589(C=C), 1488(N=N), 822(C–Cl), 468(OH, Enol). ^{1}HNMR (300 MHz, DMSO-d_6): δ ppm; 11.64 (s, 1H, NH) 10.41 (s, 1H, OH), 8.50 (s, 1H, CH=N), 8.07 (s, 1H, CH=C), 7.88–6.95 (m, 11H, Ar–H). ^{13}C-NMR (100 MHz, DMSO-d_6)): δ ppm; 174.4, 161.0, 158.6, 151.3, 145.4(2× C), 145.0, 133.0, 132.8(2× C), 130.2(2× C), 126.5(2 × C), 125.5(2 × C), 124.8, 124.7,123.5, 120.9, 118.4, 118.6, 116.8. MS (*m*/*z*, %): 496 (M^+, 12). Elemental analysis: calcd: C, 55.66; H, 3.05; Cl, 14.28; N, 14.11; S, 6.46; found: C, 55.53; H, 3.00; Cl, 14.08; N, 14.07; S, 6.33.

*2-(4-Chlorobenzylidene)hydrazinylidene)-5-(2-hydroxy-5-(p-tolyldiazenyl)benzylidene)thiazolidin-4-one (**4b**)[Cl/Me dye].* Red crystals, yield 70%, m.p. 277–280 °C. FTIR (cm^{-1}); 3480(OH), 3250(NH), 3030(CH)Ar, 2775(CH)Al, 1682(C=O), 1632 (C=N), 1591(C=C), 1488(N=N). ^{1}HNMR (300 MHz, DMSO-d_6): δ ppm; 9.92 (s, 1H, NH), 9.15 (s, 1H, OH), 8.50 (s, 1H, CH=N), 8.10 (s, 1H, CH=C), 7.85–6.90 (m, 11H, Ar–H), 2.42 (s, 3H, CH_3). ^{13}C-NMR (75 MHz, DMSO-d_6): δ ppm; 168.0, 163.6, 160.9, 150.5, 145.7(2× C), 145.3, 141.8, 133.0, 130.4(2× C), 128.8(2× C), 125.5(2× C), 123.1, 122.9(2× C), 121.4, 119.3, 117.0, 116.9, 116.6, 21.0. MS (*m*/*z*, %): 475 (M^+, 40). Elemental analysis: calcd: C, 60.57; H, 3.81; Cl, 7.45; N, 14.71; S, 6.74; found: C, 60.45; H, 3.66; Cl, 7.32; N, 14.63; S, 6.68.

*2-(Benzylidene)hydrazinylidene)-5-(5-(4-chlorophenyl)diazenyl)-2-hydroxybenzylidene)thiazolidin-4-one (**5a**)[H/Cl dye].* Red crystals, yield 89%, m.p. 288–290 °C. FTIR (cm^{-1}); 3470(OH), 3236(NH), 3061(CH)Ar, 2777(CH)Al, 1682(C=O), 1637(C=N), 1590(C=C), 1483(N=N), 833(C–Cl). ^{1}H-NMR (300 MHz, DMSO-d_6): δ ppm; 12.19 (s, 1H, NH), 10.36 (s, 1H, OH), 8.53 (s, 1H, CH=N), 8.10 (s, 1H, CH=C), 7.97–6.96 (m, 12H, Ar–H). ^{13}C-NMR (75 MHz, DMSO-d_6): δ ppm; 167.8, 160.5, 159.9, 157.5, 150.5, 144.8, 135.4, 133.9, 131.1, 129.6(2 × C), 128.9(2 × C), 128.3, 127.8(2 × C), 126.8(2 × C), 123.9, 122.9, 122.7, 121.5, 116.7. MS (*m*/*z*, %): 461 (M^+, 12). Elemental analysis: calcd: C, 59.80; H, 3.49; Cl, 7.67; N, 15.16; S, 6.94; found: C, 59.56; H, 3.42; Cl, 7.15; N, 15.09; S, 6.75.

*2-(Benzylidene)hydrazinylidene)-5-(2-hydroxy-5-(p-tolyldiazenyl)benzylidene)thiazolidin-4-one (**5b**)[H/Me dye].* Red crystals, yield 77%, m.p. 287–290 °C. FTIR (cm^{-1}); 3649(OH), 3160(NH), 3060(CH)Ar, 2920(CH)Al, 1676(C=O), 1638(C=N), 1589(C=C), 1500(N=N), 468(OH, Enol). ^{1}HNMR (300 MHz, DMSO-d_6): δ ppm; 12.03 (s, 1H, NH), 9.20 (s, 1H, OH), 8.54 (s, 1H, CH=N), 8.09 (s, 1H, CH=C) 7.92–7.14 (m, 12H, Ar–H), 2.42 (s, 3H, CH_3). ^{13}C-NMR (75 MHz, DMSO-d_6): δ ppm; 167.6, 159.9, 157.5, 149.9, 145.0, 141.2, 134.0, 131.1, 130.6, 130.3, 129.9, 128.9, 128.4, 128.3, 127.9, 127.2, 123.1, 122.3, 121.7, 121.3, 120.7, 120.6, 116.5, 21.1. MS (*m*/*z*, %): 441 (M^+, 46). Elemental analysis: calcd: C, 65.29; H, 4.34; N, 15.86; S, 7.26. Found: C, 65.14; H, 4.22; N, 15.73; S, 7.12.

*5-(5-(4-Chlorophenyl)diazenyl)-2-hydroxybenzylidene)-2-(4-methoxybenzylidene)hydrazinylidene) thiazolidin-4-one (**6a**)[MeO/Cl dye].* Yellow crystals, yield 78%, m.p. 302–304 °C. FTIR (cm^{-1}); 3490(OH), 3200(NH), 3066(CH)Ar, 2767(CH)Al, 1681(C=O), 1644(C=N), 1591(C=C), 1512(N=N), 828(C–Cl), 465(OH, Enol). ^{1}HNMR (300 MHz, DMSO-d_6): δ ppm; 12.31 (s, 1H, NHCO/N=C–OH), 10.36 (s, 1H, OH), 8.44 (s, 1H, CH=N), 8.09(CH=C), 7.96–7.01 (m, 11H, Ar–H), 3.82 (s, 3H, OCH_3). ^{13}C-NMR (75 MHz, DMSO-d_6): δ ppm; 161.6, 160.3, 158.3, 157.8, 157.3, 150.5, 145.7, 136.2, 135.3, 134.4, 131.6, 130.8, 129.6, 128.1, 126.5, 124.0, 123.4, 123.1, 123.0, 122.7, 121.5, 116.7, 114.8, 55.4. MS (*m*/*z*, %): 491 (M^+, 34). Elemental analysis: calcd: C, 58.60; H, 3.69; Cl, 7.21; N, 14.24; S, 6.52; found: C, 58.43; H, 3.50; Cl, 7.16; N, 14.21; S, 6.35.

*5-(2-Hydroxy-5-(p-tolyldiazenyl)benzylidene)-2-(4-methoxybenzylidene)hydrazinylidene)thiazolidine-4-one (**6b**)[MeO/Me dye].* Red crystals, yield 77%, m.p. 298–300 °C. FTIR (cm^{-1}); 3400(OH), 3200(NH), 3062(CH)Ar, 2762(CH)Al, 1682(C=O), 1640(C=N), 1593(C=C), 1511(N=N), 463(OH, Enol). ^{1}H-NMR (300 MHz, DMSO-d_6): δ ppm; 12.54 (s, 1H, NHCO), 10.35 (s, 1H, OH), 8.47 (s, 1H, CH=N), 8.09 (s, 1H, CH=C), 7.91–7.03 (m, 11H, Ar–H), 3.84 (s, 3H, OCH_3), 2.42 (s, 3H, CH_3). ^{13}C-NMR (75 MHz, DMSO-d_6): δ ppm; 167.3, 161.6, 159.7, 158.1, 157.2, 152.8, 149.9, 145.0, 141.2, 129.9(2× C), 129.6, 126.7, 126.5, 123.2, 122.8, 122.3(2× C), 122.0, 121.3, 116.5, 114.4(2× C), 55.3, 21.0. MS (*m*/*z*, %): 471 (M^+, 31). Elemental analysis: calcd: C, 63.68; H, 4.49; N, 14.85; S, 6.80; found: C, 63.46; H, 4.43; N, 14.67; S, 6.63.

Biological activity

Cell viability and cytotoxicity assay. Normal human skin fibroblasts (HSF), the human breast cancer epithelial cell line (MDA), and the human liver cancer cell line (HepG2) were purchased from VACCERA Egypt and obtained from the American Type Culture Collection (ATCC). HSF and MDA cells were cultured in Dulbecco's Modified Eagle Medium (DMEM) (Lonza, USA), supplemented with 10% fetal bovine serum (FBS) and 1% penicillin–streptomycin, while HepG2 cells were cultured in Roswell Park Memorial Institute (RPMI-1640) medium (Lonza, USA), also supplemented with 10% FBS (GIBCO BRL, USA), at 37 °C under a humidified atmosphere with 5% CO_2. The cells were plated in 96-well plates (5×10^3 cells per well) and subsequently exposed to different concentrations of synthetic compounds (**4–6a,b**), ranging from 1 to 1000 μg mL^{-1} for HSF cells and 1 to 100 μg mL^{-1} for the cancer cell lines. After 48 hours of incubation, cell viability was assessed using the "MTT" (1-(4,5-dimethylthiazol-2-yl)-3,5-diphenyl formazan, thiazolyl blue formazan) assay with some modifications.[24,25] The CC_{50} and IC_{50} values, representing the concentration at which the synthetic compounds (**4–6a,b**) inhibit 50% of cell viability, were calculated using GraphPad Prism 8.0 software. The selectivity index (SI) was determined by calculating the ratio of the CC_{50} for normal cells (HSF) to the IC_{50} values for cancer cells. Additionally, morphological changes in cancer cells were examined using inverted phase-contrast microscopy with the Zoe Fluorescent Cell Imager (Bio-Rad, California). Each experiment was performed in triplicate and compared to 5-fluorouracil (5-FU) as the reference chemotherapeutic agent and untreated control cells.[26,27]

Fluorescence microscopy examination. Acridine orange/ethidium bromide (AO/EB) dual staining was employed to

observe morphological indicators of early and late apoptosis. MDA and HepG2 cells were plated in 12-well plates and incubated overnight to allow for adhesion. After 48 hours of treatment with the compounds at IC_{50} concentrations, the cells were washed twice with phosphate-buffered saline (PBS). Subsequently, 10 μL of AO/EB dye solution was added, and the cells were incubated for 15 minutes. Following incubation, the cells were washed again with PBS and observed under a Zoe Fluorescent Cell Imager (Bio-Rad, California) using fluorescence microscopy.[26–28]

Scratch assay. The scratch assay was employed to evaluate cell migration in both cancer cell lines following various treatments. MDA and HepG2 cells were seeded at a density of 1×10^5 cells per well in 12-well plates. Once the cells reached 90% confluence, a scratch was made using a sterile pipette tip to create a wound, and the cells were washed with PBS to remove damaged cells. The medium was replaced with medium containing 5% fetal bovine serum. The cells were treated with different compounds and monitored for 48 hours. The wound area was quantified, and the wound area percentage was calculated by comparing the wound area at 48 hours to the initial wound area at 0 hours for each group. Each well was photographed using a bright field inverted microscope. Each experiment was performed in triplicate and compared to untreated control cells.[26–29]

Gene expression assessment. Real-time PCR approach was utilized as a quantitative estimation process to determine the influence of the synthetic derivatives on the expression levels of some genes, such as matrix metalloproteinases MMP-2 and MMP-9 genes in the treated MDA and HepG-2 cancer cell lines. Total RNAs from untreated and treated MDA and HepG-2 cell lines at IC_{50} dose of each synthetic derivatives were separated and extracted using the prtocol of Gene JET RNA Purification Kit (Thermo Scientific, USA). Using the synthesis of cDNAs following the manual of the cDNA Synthesis Kit (Thermo Scientific, USA), qPCR was performed *via* the SYBR green master mix and using the specific forward/reverse primers of 5′-AGACAGTGGATGATGCCTTTGC-3′/5′-GGAGTCCGTCCTTACCGTCAAA-3′ for MMP-2 gene and 5′-CTGCGTATTTCCATTCATC-3′/5′-CCTTGGGTCAGGTTTAGAG-3′ for MMP-9 gene. The fold alteration of each expression level for the treated MDA and HepG-2 cells with the synthetic derivatives was assessed using the $2^{-\Delta\Delta CT}$ equation as related to untreated cells.[30,31]

Docking study

The default docking protocol of MOE 2014 software was applied according to the methodology described in the supplementary data.[32,33]

Statistical analysis

All experiments were performed in triplicate, and the results were statistically analyzed. Data were expressed as mean ± standard error (SEM). Statistical significance was determined using two-way analysis of variance (ANOVA) followed by Sidak's multiple comparisons test, with a significance threshold set at

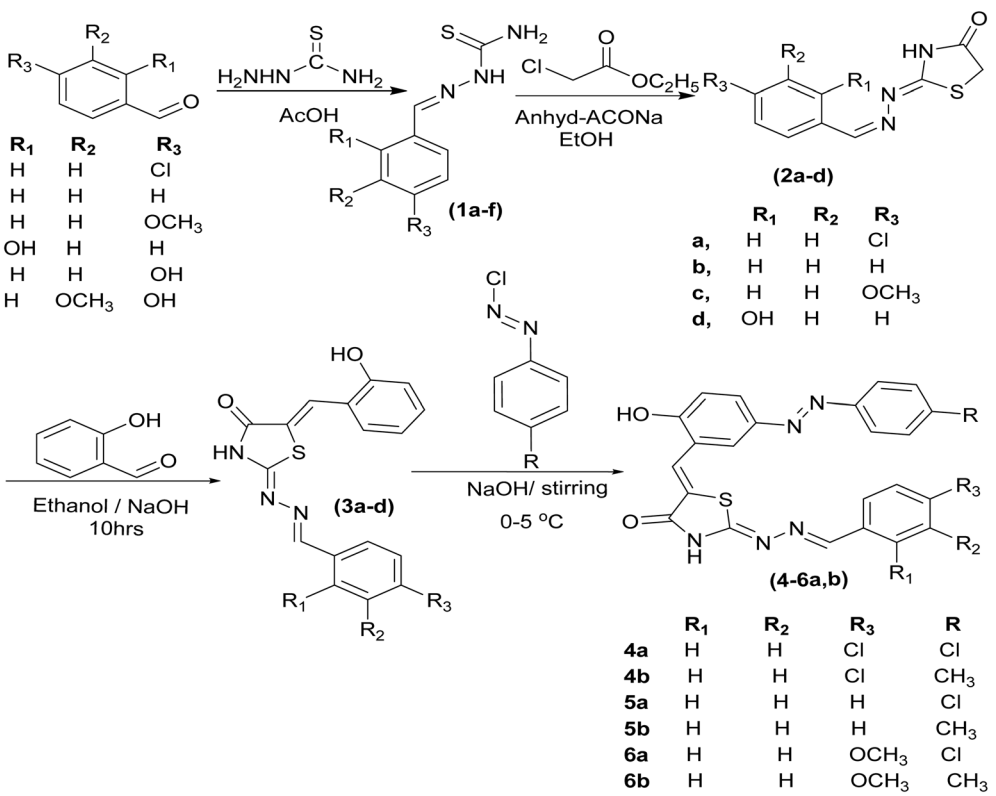

	R_1	R_2	R_3
	H	H	Cl
	H	H	H
	H	H	OCH_3
	OH	H	H
	H	H	OH
	H	OCH_3	OH

	R_1	R_2	R_3
a,	H	H	Cl
b,	H	H	H
c,	H	H	OCH_3
d,	OH	H	H

	R_1	R_2	R_3	R
4a	H	H	Cl	Cl
4b	H	H	Cl	CH_3
5a	H	H	H	Cl
5b	H	H	H	CH_3
6a	H	H	OCH_3	Cl
6b	H	H	OCH_3	CH_3

Scheme 1 Synthetic routes to thiosemicarbazones (**1a–f**), thiazolidine derivatives (**2a–d**), chalcones (**3a–c**) and diazenyl-chalcones (**4–6a,b**).

$p < 0.05$. Additionally, nonlinear regression analysis was performed on the normalized transformed data to fit the dose–response curves.

Results and discussion

Chemistry

The development of novel compounds with potential anticancer activity remains a major focus due to the persistent need for selective and effective therapeutic agents. Molecular hybridisation, which combines pharmacologically active fragments from different molecules, offers a strategy for generating hybrid scaffolds with enhanced biological properties compared with their individual precursors.

Following this approach, a series of 2-[4-substituted-benzylidene]-hydrazine-1-carbothioamide derivatives (**1a–f**) was synthesised by condensing various aromatic aldehydes—4-chlorobenzaldehyde, benzaldehyde, 4-methoxybenzaldehyde, 2-hydroxybenzaldehyde, 4-hydroxybenzaldehyde, and 4-hydroxy-3-methoxybenzaldehyde—with thiosemicarbazide in ethanol using a catalytic amount of acetic acid (Scheme 1).[34,35] The structures were confirmed by FTIR, ^{1}H NMR, and ^{13}C NMR spectroscopy. In the ^{1}H NMR spectra, N–H protons appeared at 11.21–12.02 ppm, CH═N protons at 8.01–8.39 ppm, and NH_2 protons at 7.79–8.07 ppm. The ^{13}C NMR spectra showed thioxo (C═S) carbons at 177.16–178.09 ppm, consistent with the proposed structures.

The thiosemicarbazone intermediates **1a–d** was cyclised with ethyl chloroacetate in ethanol in the presence of anhydrous sodium acetate under reflux to yield 2-(4-substituted-benzylidene)-hydrazinylidene-thiazolidin-4-one derivatives (**2a–d**).[36–38] This step generated the thiazolidin-4-one ring, a key pharmacophoric element for subsequent hybridisation. Spectroscopic analysis indicated tautomeric mixtures of ketone and enol forms. In ^{1}H NMR spectra, the SCH_2 protons of the thiazolidinone ring appeared as singlets at 3.82–3.96 ppm, while CH═N protons resonated at 8.39–9.43 ppm. The ^{13}C NMR spectra exhibited characteristic signals for the carbonyl carbon (C═O) at 173.93–174.36 ppm and the methylene carbon (CH_2) at 33.03–33.42 ppm.

Next, a Claisen–Schmidt condensation of **2a–d** with salicylaldehyde in ethanol containing NaOH produced the chalcone

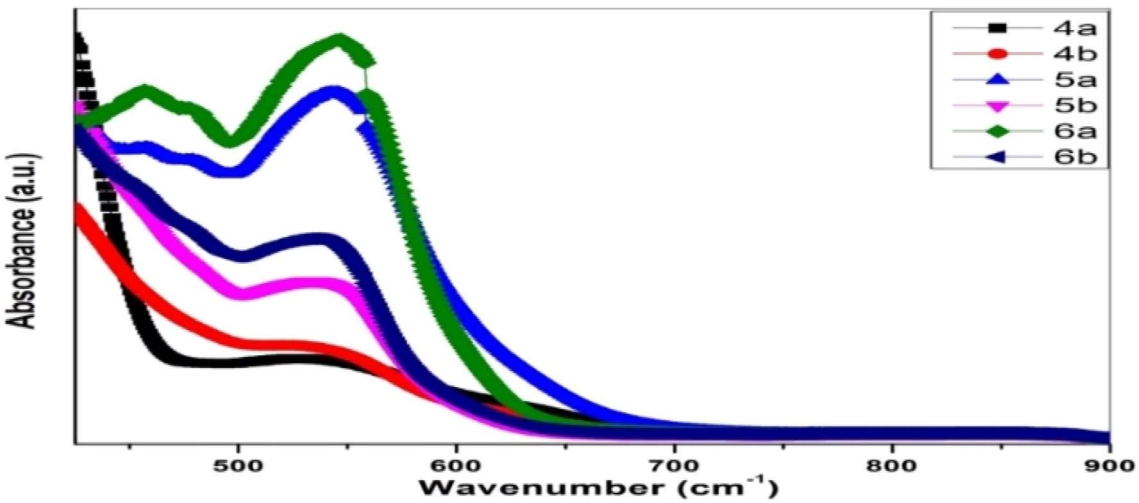

Fig. 1 UV-visible absorption spectra for diazenyl chalcones disperse dyes incorporating 2-arylidene hydrazineylidene thiazole.

Table 1 The CC_{50}, IC_{50} (μM), and selectivity index of the tested compounds against MDA and HepG2 cancerous cell lines as compared to normal HSF cell line[a]

	HSF	HepG2		MDA	
Compound	CC_{50}	IC_{50}	SI	IC_{50}	SI
4a	707.07 ± 7.39	574 ± 2.57	1.23	331.72 ± 4.06	2.14
4b	794.74 ± 4.66	31.66 ± 2.91	25.09	37.71 ± 3.13	21.08
5a	806.72 ± 7.04	27.92 ± 2.33	28.89	26.16 ± 3.81	30.84
5b	611.56 ± 5.46	24.17 ± 2.67	34.68	24.56 ± 2.28	34.14
6a	866.6 ± 6.61	22.26 ± 2.79	38.93	23.89 ± 3.37	36.27
6b	973.25 ± 4.83	137.71 ± 4.37	7.07	97.75 ± 4.09	9.96
5-FU	37.83 ± 3.11	32.14 ± 2.72	1.18	27.91 ± 1.64	1.36

[a] Statistical analysis was performed using two-way ANOVA followed by Sidak's multiple comparisons test, showing no significant differences ($p > 0.05$) in selectivity index (SI) between MDA and HepG2 cells across all conditions.

derivatives **3a–d**, forming 2-(4-substituted-benzylidene) hydrazinylidene-5-(2-hydroxybenzylidene)thiazolidin-4-one hybrids.[24,30,39,40] These compounds incorporate both thiazolidinone and hydroxybenzylidene motifs, enhancing planarity and conjugation. Spectroscopic characterization confirmed their structures and Z-geometry: the C=CH methine proton appeared at 7.88–8.51 ppm, and the absence of methylene proton signals from the thiazolidinone ring, with the phenolic OH proton observed as a singlet at 10.25–10.66 ppm. IR, ^{13}C NMR, mass spectrometry, and elemental analysis further supported structural assignment.

Finally, diazenyl chalcone derivatives **4–6a,b** was obtained by diazotization of the corresponding aromatic amines followed by electrophilic coupling with chalcone intermediates **3a–c**. This sequence efficiently introduced the azo (–N=N–) linkage onto the 2-(4-substituted-benzylidene)hydrazinylidene-5-(2-hydroxybenzylidene)thiazolidin-4-one scaffold, affording hybrid molecules with extended π-conjugation and enhanced structural rigidity.

Spectroscopic data confirmed the proposed structures. The IR spectra of compounds **4–6a,b** exhibited characteristic absorptions for N=N at 1480–1515 cm^{-1}, C=O at 1676–1682 cm^{-1}, and broad O–H bands at 3300–3649 cm^{-1}. Their ^{1}H NMR spectra showed aromatic proton resonances in the region of 6.96–7.91 ppm. As a representative example, compound **6b** displayed IR bands at 1682 cm^{-1} (C=O),

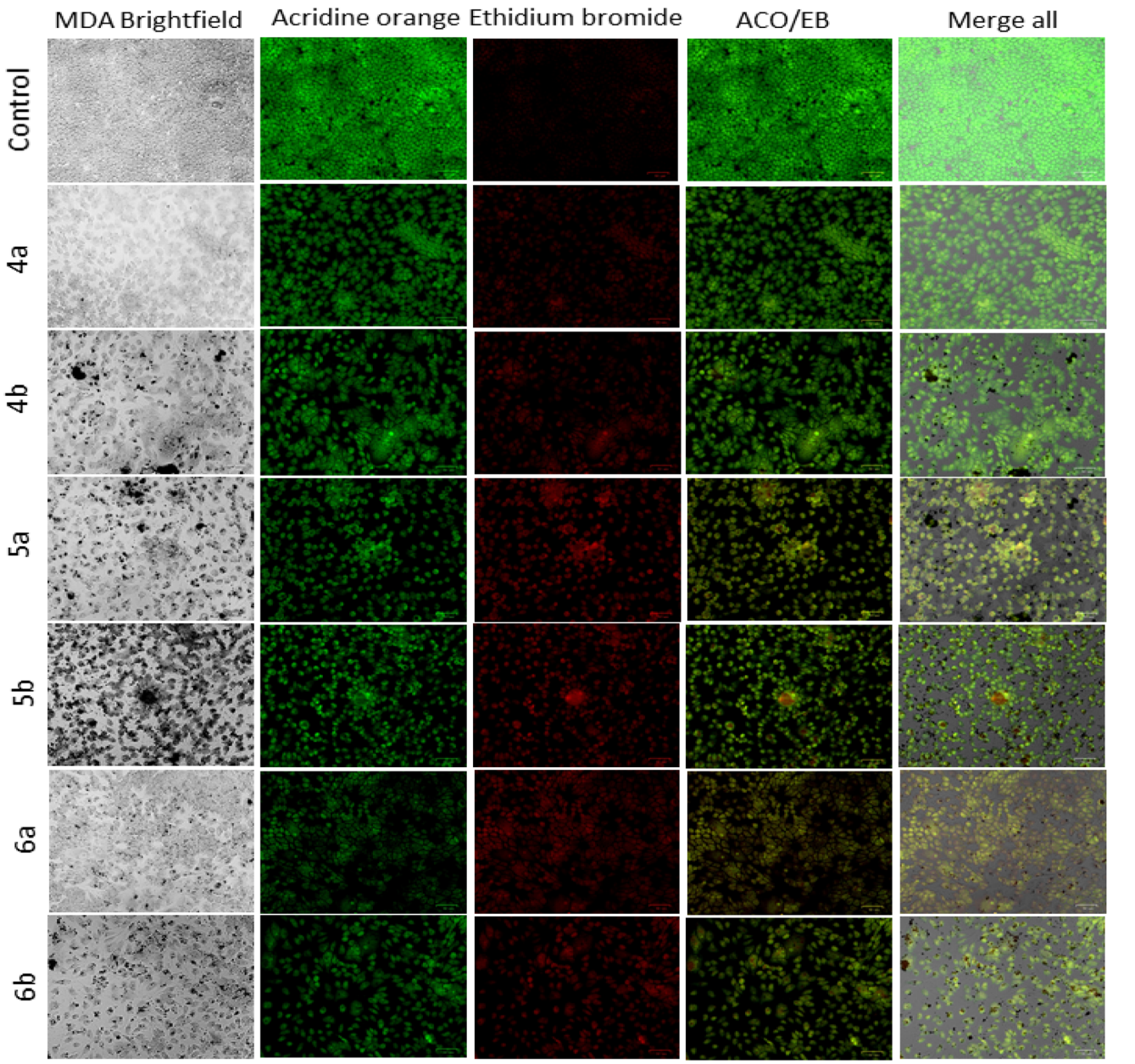

Fig. 2 Fluorescent microscopy analysis of MDA cells treated with synthetic compounds (**4–6a,b**) and stained with acridine orange/ethidium bromide (AO/EB).

1640 cm^{-1} (C═N), and 1511 cm^{-1} (N═N). Its ^1H NMR spectrum featured singlets at 10.35, 8.47, 8.09, 3.84, and 2.42 ppm, corresponding to OH, CH═N, C═CH, OCH_3, and CH_3 protons, respectively, along with a downfield singlet at approximately 12.65 ppm assigned to the NH–CO tautomeric form. The ^{13}C NMR spectrum of **6b** further supported the structure, giving prominent resonances at 167.37 ppm (C═O), 161.60 ppm (C–OH), 55.38 ppm (OCH_3), and 21.03 ppm (CH_3).

Mass spectral analysis of **6b** showed a molecular ion at *m*/*z* 471 (M^+, 31%) consistent with $C_{25}H_{21}N_5O_3S$, along with a base peak at *m*/*z* 468 (100%) corresponding to $C_{25}H_{18}N_5O_3S$, confirming the proposed molecular framework. A complete set of correlation data is provided in the SI.

Overall, this synthetic strategy [Scheme 1] afforded a series of diazenyl chalcone hybrids incorporating the 2-arylidene hydrazinylidene thiazolidin-4-one core. These molecules integrate multiple pharmacophores—including the chalcone α,β-unsaturated carbonyl system, the thiazolidinone moiety, the hydroxybenzylidene group, and the azo linkage—features that are expected to act synergistically to enhance biological properties, particularly anticancer potential.

Visible spectroscopy

The structures of the synthesised diazenyl chalcones were validated using the UV-Vis absorption spectra (4–6a,b). In Witt's

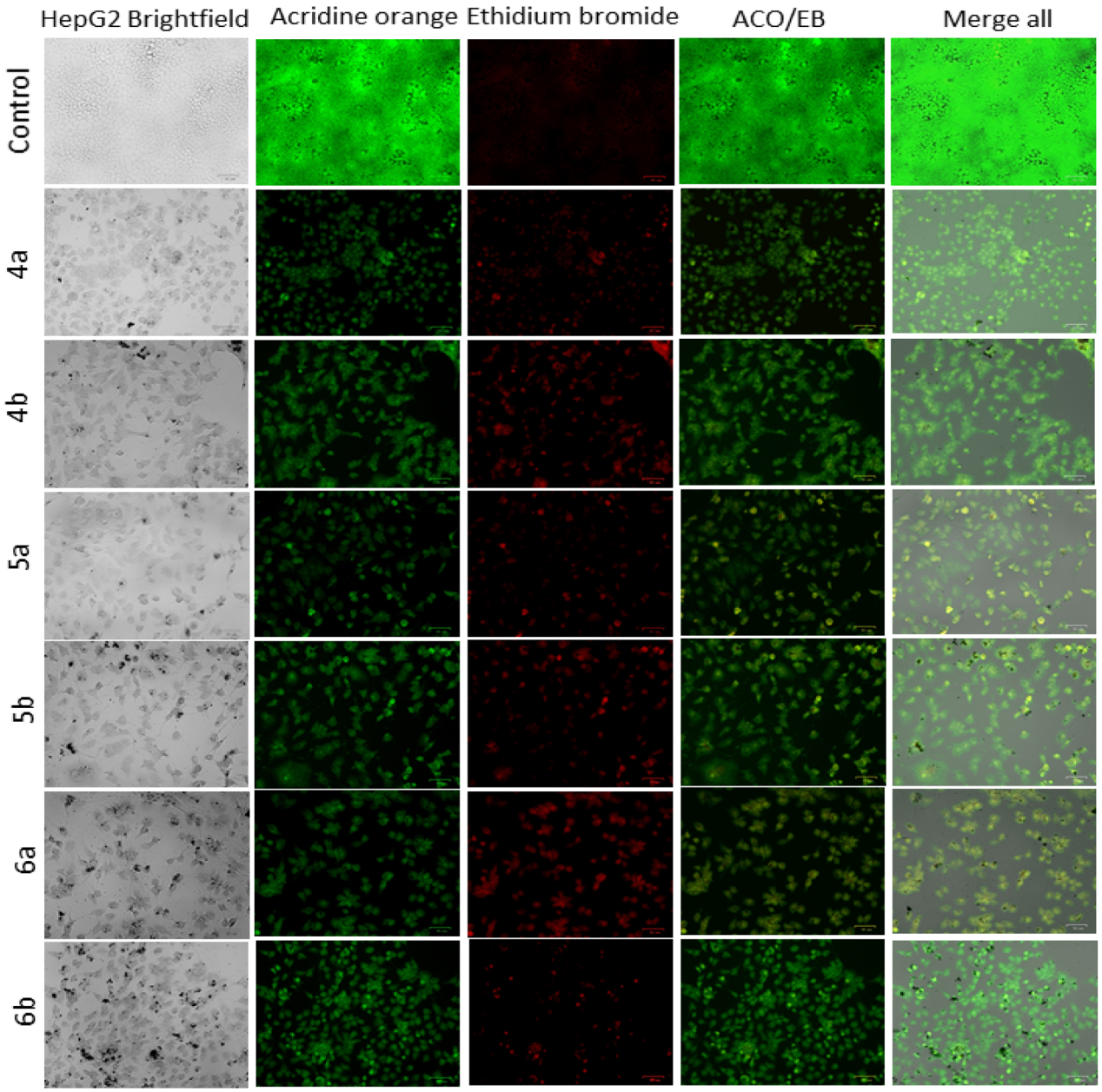

Fig. 3 Fluorescent microscopy analysis of HepG2 cells treated with synthetic compounds (**4–6a,b**) and stained with acridine orange/ethidium bromide (AO/EB).

chromophore theory, bathochromic shifts are caused by the modulation of π-conjugation by substituents that donate electrons (such as NHCO CH_3, OCH_3 or CH_3) on one aromatic ring and by substituents that withdraw electrons (such as NO_2, CN, or halogens) on the other. To find the maximum absorption wavelengths (λ_{max}), the spectra were recorded in DMSO at room temperature in this investigation. Fig. 1 shows the predicted visible absorption spectra of the six dyes. Dye **4a** (Cl/Cl) and dye **4b** (Cl/CH_3) are highly visible-light absorbers. When compared to dye **4a**, dye **4b** exhibits a more pronounced red shift. The methyl group on the diazenyl-benzylidene molecule donates electrons, reducing the energy required for the electronic transition. There is a clear absorption band at about 540 nm for dye **5a** (H/Cl) and a broader and less intense band for dye **5b** (H/CH_3), which indicates less conjugation because of the methyl group. There is more complexity in the spectra of dyes **6a** (OCH_3/Cl) and **6b** (OCH_3/CH_3). The absorption peak at approximately 550 nm is clearly visible in compound **6a**, whereas a wider, redder band centred at about 538 nm is seen in dye **6b**, suggesting weaker electronic transitions. Generally, changes in the substituents on the benzylidene units greatly impact the complexity, location, and strength of the visible absorption bands. Due to the increased conjugation between the diazenyl group and the thiazolidin-4-one core, the 4-chlorophenyl derivatives (Cl/Cl, H/Cl, OCH_3/Cl) exhibit stronger, blue-shifted transitions. Because the electron-donating methyl group reduces conjugation effectiveness, the *p*-tolyl derivatives (Cl/CH_3, H/CH_3, OCH_3/CH_3) show weaker, red-shifted absorptions. These spectral features highlight the synthesised dyes' potential as wavelength-selective spectroscopic probes and dye-sensitised solar cell possibilities.

Biological activity

We assessed the cell viability of synthetic compounds (4–6a,b) using the MTT assay on normal HSF cells, MDA (breast cancer), and HepG2 (liver cancer) cells (Table S1 and Fig. S7). Most compounds exhibited little to no toxicity on normal cells at concentrations of 100 μg mL^{-1} or lower. Furthermore, except for compound **4a**, all compounds demonstrated anticancer activity at concentrations below the safe dose. No significant differences in cytotoxicity were observed between MDA and HepG2 cells, though compounds **5a**, **5b**, and **6a** showed the highest selectivity indices, as presented in Table 1. The selectivity indices for **5a**, **5b**, and **6a** were 30.84, 34.14, and 36.27 against MDA, and 28.89, 34.68, and 38.93 against HepG2 cells, respectively. Interestingly, Table 1 indicates that the compounds **5a**, **5b**, and **6a** exhibited more anticancer activity against HepG2 cells with IC_{50} values of 27.92 ± 2.33,

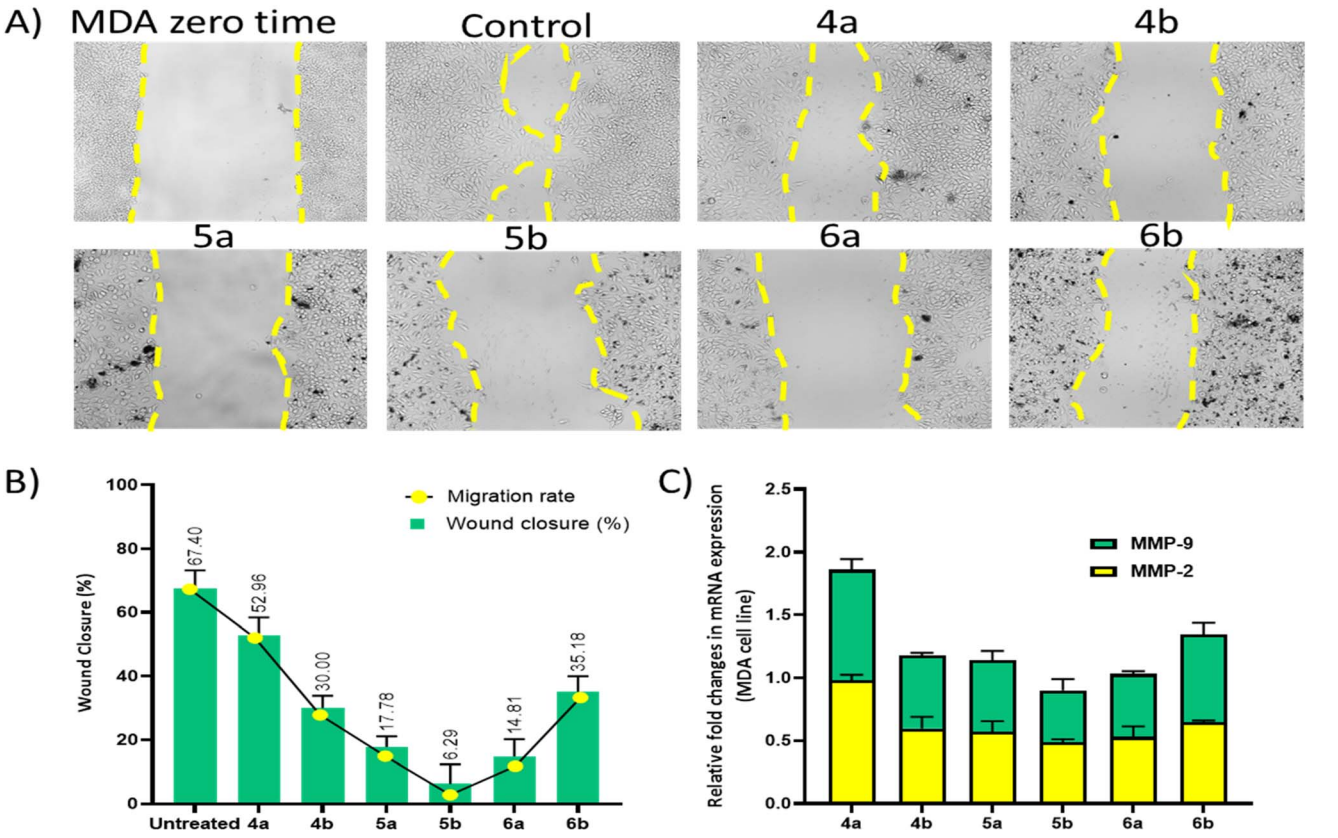

Fig. 4 (A) Microscopic view of the cell migration inhibition assay of the MDA cell line after 48 hours. (B) Quantitative analysis of the wound area by calculating the wound closure percentage and migration rate after 48 hours, compared to the initial time (0 hours). (C) Relative fold change in the gene expression of MMP-2 and MMP-9 in cells treated with synthetic compound (**4–6a,b**) in MDA. All assays were conducted in triplicate, and the results are expressed as mean ± SEM. MMP: matrix metalloproteinase.

24.17 ± 2.67 and 22.26 ± 2.79 μM, respectively, potent than 5-FU (32.14 ± 2.72 μM). Furthermore, compounds **5a**, **5b**, and **6a** showed IC_{50} value of 26.16 ± 3.81, 24.56 ± 2.28 and 23.89 ± 3.37 μM more than 5-FU (27.91 ± 1.64 μM) as presented in Table 1. Microscopic examination revealed noticeable changes in MDA (Fig. 2) and HepG2 cells (Fig. 3), including cell shrinkage and nuclear condensation, particularly at higher concentrations, indicating apoptosis induction. Fluorescence microscopy using acridine orange/ethidium bromide (AO/EB) staining confirmed apoptosis, with viable cells exhibiting green fluorescence and apoptotic cells displaying greenish-yellow to red fluorescence due to membrane disruption. An ideal anticancer compound exhibits cytotoxic effects on cancer cells at low concentrations (low IC_{50}) while maintaining minimal toxicity to normal cells at higher concentrations (high CC_{50}), resulting in a high selectivity index ($SI = CC_{50}/IC_{50}$). The selectivity index is a well-established parameter used to assess the therapeutic window and *in vitro* efficacy of anticancer agents.[38]

Bright field images show the viability of MDA cells after treatment with varying concentrations of synthetic compounds (**4–6a,b**). Fluorescent images display live cells in green (stained with AO) and dead or apoptotic cells in red (stained with EB). The merged AO/EB images distinguish live cells (green), early apoptotic cells (yellow/orange), and late apoptotic cells (red). The final column in the figure represents a merged image combining all fluorescence channels, including acridine orange (green) and ethidium bromide (red), overlaid with the bright-field image.

Bright field images show the viability of HepG2 cells after treatment with varying concentrations of synthetic compounds (**4–6a,b**). Fluorescent images display live cells in green (stained with AO) and dead or apoptotic cells in red (stained with EB). The merged AO/EB images distinguish live cells (green), early apoptotic cells (yellow/orange), and late apoptotic cells (red). The final column merges all channels, providing a comprehensive overview of cell viability and structural integrity across the different treatments.

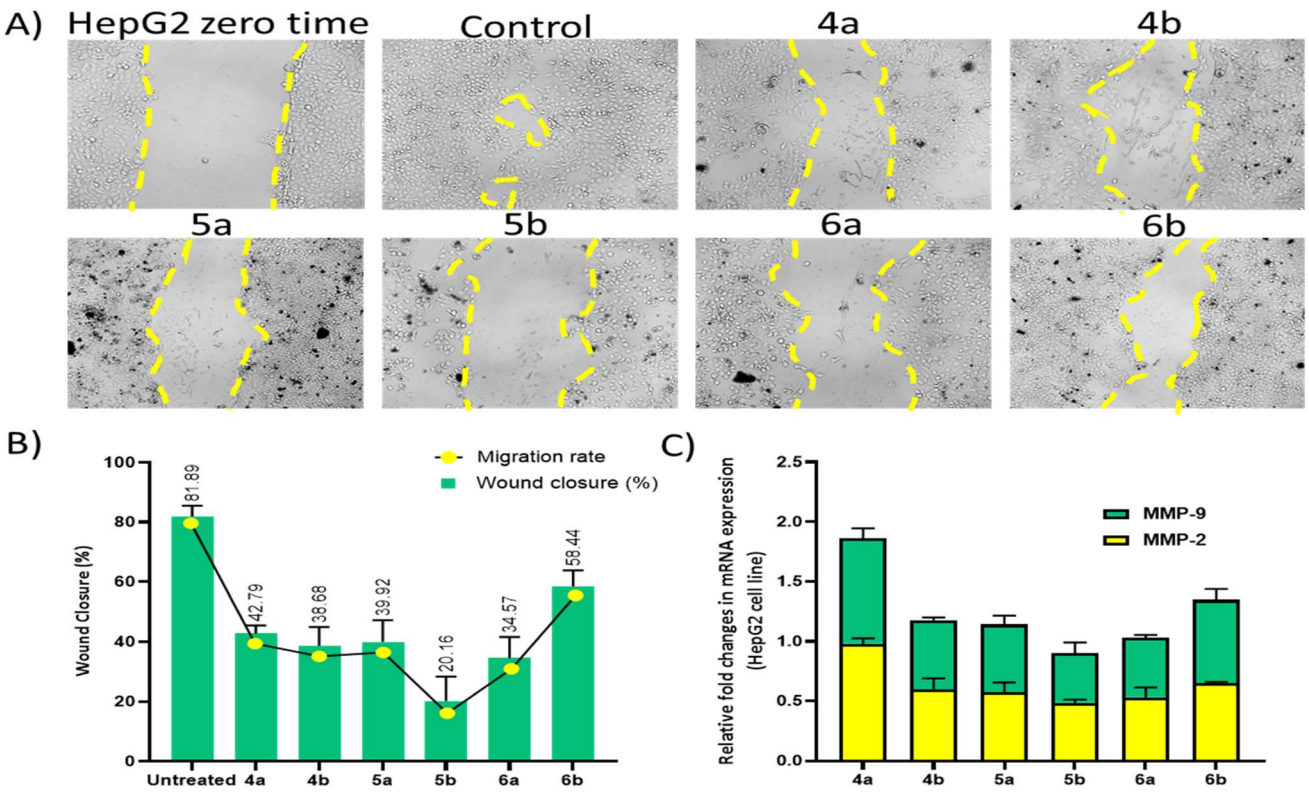

Fig. 5 (A) Microscopic view of the cell migration inhibition assay of the HepG2 cell line after 48 hours. (B) Quantitative analysis of the wound area by calculating the wound closure percentage and migration rate after 48 hours, compared to the initial time (0 hours). (C) Relative fold change in the gene expression of MMP-2 and MMP-9 in cells treated with synthetic compounds (**4–6a,b**) in HepG-2. All assays were conducted in triplicate, and the results are expressed as mean ± SEM. MMP: matrix metalloproteinase.

Table 2 Binding free energies of the new derivatives against MMP-2 and MMP-9 receptors

Comp. ID	Ligand	4a	4b	5a	5b	6a	6b
1HOV score (kcal mol^{-1})	−33.73	−25.19	−22.80	−14.98	−29.72	−32.27	−32.67
1GKC score (kcal mol^{-1})	−14.95	−24.32	−23.76	−23.38	−23.70	−23.30	−21.54

Our study evaluated the migration inhibitory effects of synthetic substances on MDA and HepG2 cells by a wound healing experiment. Phase-contrast photographs of the wound area at IC_{50} doses demonstrated substantial migratory inhibition relative to untreated control cancer cells. The yellow dashed lines denote the wound margins at 0 and 48 hours (Fig. 4A and 5A). Compounds **5a**, **5b**, and **6a** exhibited a pronounced anti-migration effect on MDA cells, whilst compounds **5b** and **6a** displayed a comparable effect on HepG2 cells, as indicated by the minimal wound closure percentages and reduced migration rates (Fig. 4B and 5B). Additionally, gene expression study revealed that the synthetic compounds (**4–6a,b**) downregulated the expression of matrix metalloproteinases (MMP-2 and MMP-9), with the exception of compound **4a**. These enzymes are crucial facilitators of cancer cell migration and invasion. The expression of MMP-2 was diminished relative to untreated cells, indicating that the compounds exercise their anti-metastatic actions by disrupting essential pathways associated with tumor cell migration and metastasis (Fig. 4C and 5C).

Docking study

We conducted docking study in order to get insights on the affinity and binding patterns of the new designed molecules to some important enzymes highly related to cancer, especially to cell migration process. On the basis of promising biological effects of the new derivatives as inhibitors to cell migration, we suggested that Matrix metalloproteinase-2 (MMP-2) and matrix metalloproteinase-9 (MMP-9) are likely to be suitable proteins for docking study. Especially gene expression study revealed that the synthetic compounds (**4–6a,b**) downregulated the

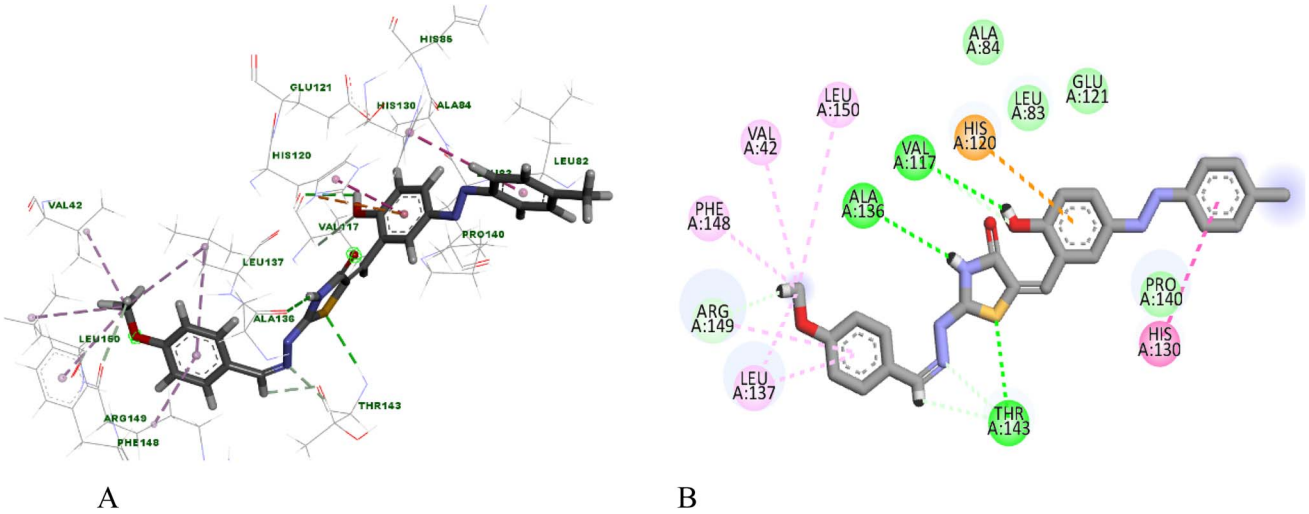

Fig. 6 Binding mode of compound **6b** to MMP-2 protein (A) 3D illustration, (B) 2D image.

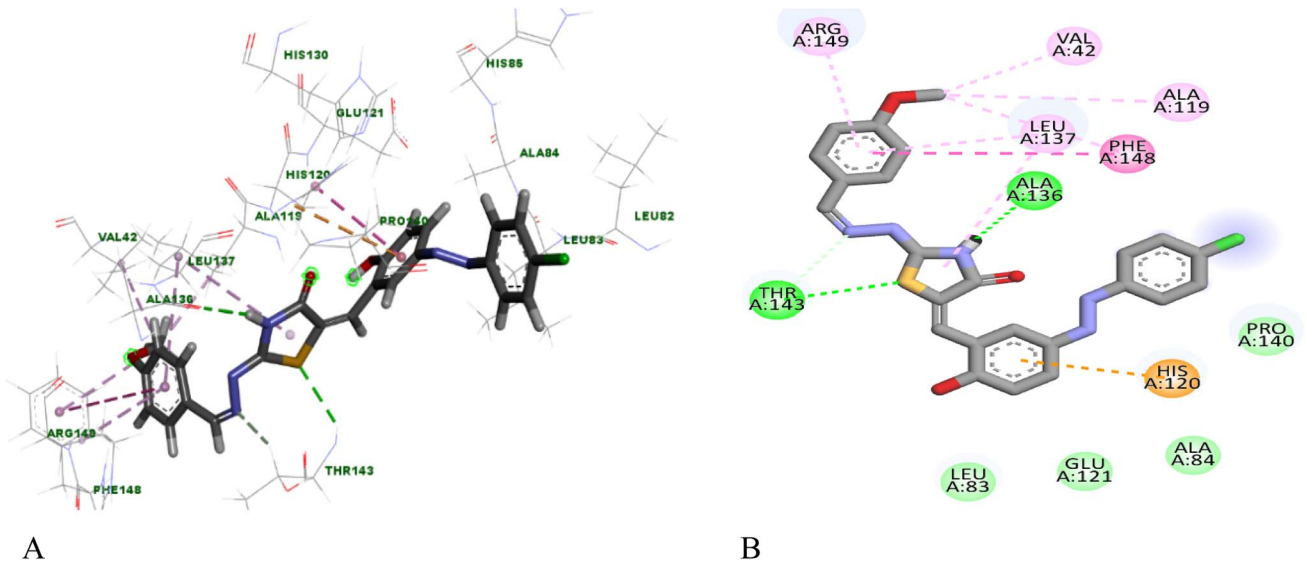

Fig. 7 Binding mode of compound **6a** to MMP-2 protein (A) 3D illustration, (B) 2D image.

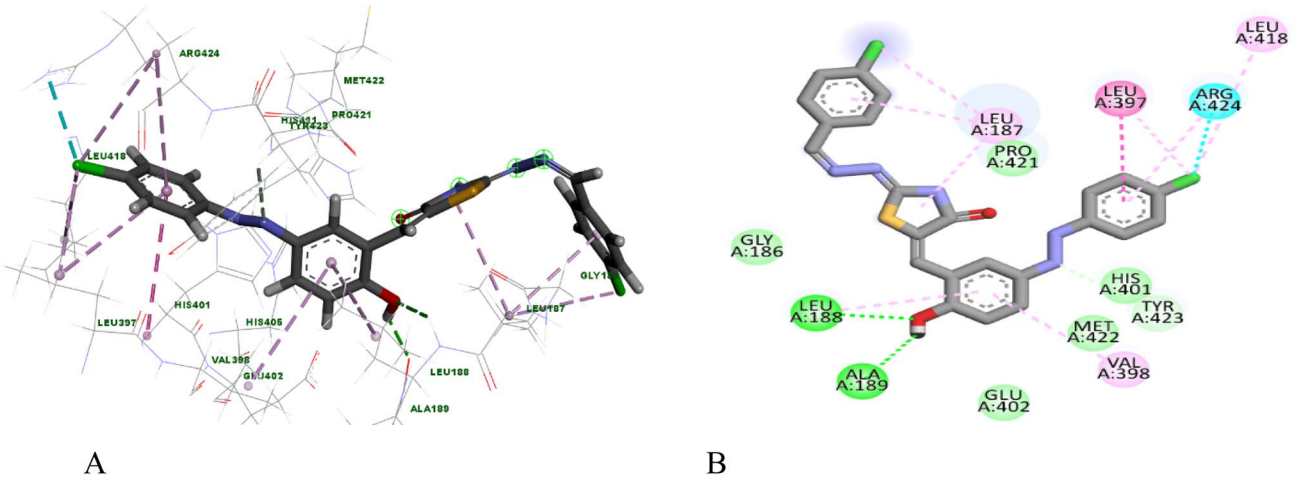

Fig. 8 Binding mode of compound **4a** to MMP-9 protein (A) 3D illustration, (B) 2D image.

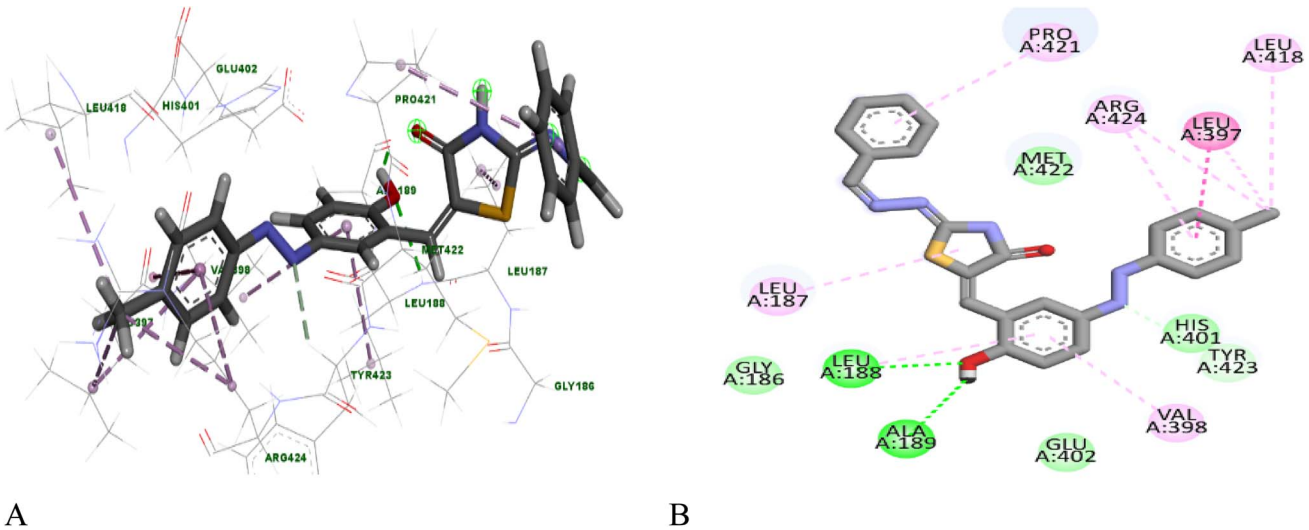

Fig. 9 Binding mode of compound **5b** to MMP-9 protein (A) 3D illustration, (B) 2D image.

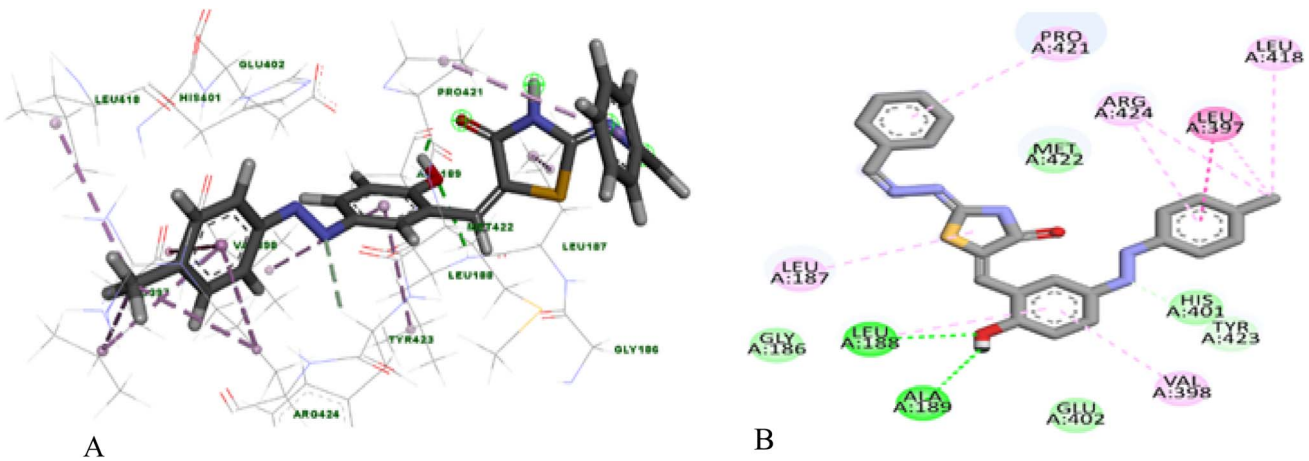

Fig. 10 Binding mode of compound **5b** to MMP-9 protein (A) 3D illustration, (B) 2D image.

expression of both MMP-2 and MMP-9. Molecular operating environment software (MOE) was used to make calculations and suggest binding free energies and binding modes according to default docking protocol. The crystal structure of the enzymes (ID: 1HOV and 1GKC for MMP-2 and MMP-9, respectively) were obtained from protein data bank website (PDB). The obtained results revealed that the new derivatives have strong affinities to both MMP-2 and MMP-9. The binding free energies of the new molecules and ligands are outlined in Table 2.

It can be noticed that the new molecules showed good affinity to MMP-2 receptor ranging from −32.67 to −14.98 kcal mol^{-1}. Compounds **6a** and **6b** showed the best results with scores (−32.67 and −32.27 kcal mol^{-1}, respectively) comparable to that of the ligand (33.73 kcal mol^{-1}). Compound **5b** came in the third order with score of −29.72 kcal mol^{-1}. Compounds **4a** and **4b** showed relatively weaker scores, while compound **5a** was far weaker than other derivatives. With respect to MMP-9 receptor, the new derivatives revealed far better scores (ranging from −24.32 to −21.54 kcal mol^{-1}) than that of the ligand (−14.95 kcal mol^{-1}). It is clear that docking scores of the new candidates are ranged from −24.32 to −21.54 kcal mol^{-1}, indicating comparable binding affinities. Compound **4a** came first with a score of −24.32 kcal mol^{-1}. Compound **6b** was the last one, while compounds **4b**, **5a**, **5b**, and **6a** were comparable to **4a**. Regarding the binding modes of the new molecules to MMP-2, different binding interactions to amino acids of the active site were obtained. Fig. 6 illustrates the binding pattern of compound **6b** to 1HOV pocket, where it formed three hydrogen bonds with Val117, Ala136, and Thr143. Additionally, it displayed a Pi–Pi interaction with His130 and a Pi–cation interaction with His 120. Moreover, it revealed hydrophobic interactions with Leu150, Val42, Phe148, and Leu137.

Binding mode of compound **6a** is illustrated in Fig. 7. It can be noticed that **6a** showed hydrogen bonds with Ala136 and Thr143. It also revealed a Pi–Pi interaction with Phe148 and a Pi–cation interaction with His120. In addition to hydrophobic interactions with Arg149, Val42, Ala119, and Leu137.

Meanwhile, the binding mode of the designed compounds to MMP-9 are represented by Fig. 8 and 9, which illustrate the interaction patterns of compounds **4a** and **5b**, respectively. We can see that compound **4a** exhibited hydrogen bonds with Ala189 and Leu188 and Pi–alkyl interactions with Val398, Leu188, Leu187, and Arg424. In addition, it revealed amide–Pi interaction with Leu397 and hydrophobic interaction with His401.

Similarly, compound **5b** showed hydrogen bonds with Leu188 and Ala189 and amide Pi stacking with Leu397. Furthermore, it displayed Pi–alkyl interactions with Val398,

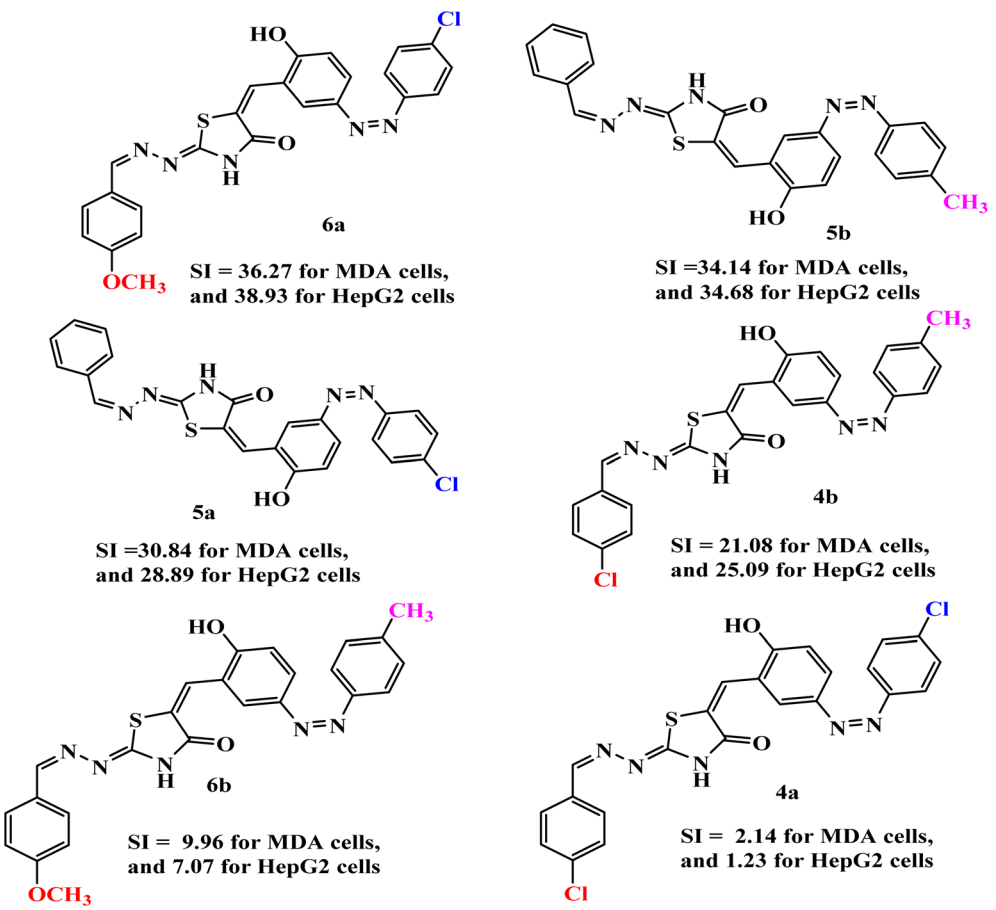

Fig. 11 Structure–activity relationship (SAR) of the synthesised azo derivatives (**4–6a,b**) showing the effect of aromatic substitution on cytotoxic selectivity. Selectivity index (SI) values against MDA-MB-231 and HepG2 cells relative to WI-38 normal cells are shown.

Leu187, Leu188, Arg424, and Pro421. In addition to hydrophobic interaction with Leu418 (see Fig. 10).

Structure–activity relationship (SAR)

Cytotoxic activity and selectivity index of the synthesised azo derivatives (**4–6a,b**) were evaluated against MDA-MB-231 and HepG2 cancer cell lines, with selectivity assessed relative to normal WI-38 cells. Table 1 shows that the biological activity of these compounds depends heavily on the nature and position of substituents on the phenyl rings. Among all synthesised derivatives, compound **6a** exhibited the highest cytotoxic selectivity, with SI values of 36.27 (MDA-MB-231) and 38.93 (HepG2). The presence of both methoxy (–OCH_3) and chloro (–Cl) substituents is what makes this activity so impressive. The chloro group increases molecular hydrophobicity and thereby improves membrane permeability, while the methoxy group contributes additional hydrophobic interactions with Val42, Ala119, and Leu137. As an electron-donating substituent, –OCH_3 also enhances π–π stacking with Phe148, collectively strengthening the ligand–protein binding affinity. On the other hand, compound **4a** had the lowest selectivity (SI = 2.14 for MDA-MB-231; 1.23 for HepG2). The presence of only a chlorine substituent reduces electronic richness and limits the variety and strength of stabilising interactions within the active site, resulting in weaker cytotoxic performance.

Compounds **4b**, **5a**, and **5b** demonstrated consistently high selectivity (SI = 21.08–34.14 for MDA-MB-231; 25.09–34.68 for HepG2). These results can be attributed to the presence of both electron-withdrawing (Cl) and electron-donating (CH_3) groups on the aromatic system. The combination of these substituents creates a balanced electronic distribution that enhances intermolecular contacts and promotes stable ligand–protein complexes.

In comparison, compound **6b** showed moderate selectivity (SI = 9.96 for MDA-MB-231; 7.07 for HepG2). The reduced activity suggests that symmetrical substitution—whether strongly electron-donating or electron-withdrawing—results in a less favourable electronic arrangement that compromises optimal binding and consequently diminishes anticancer potency.

As illustrated in Fig. 11, the SAR analysis indicates the following trends:

Mixed substituents (EDG + EWG) favour high selectivity and potency, likely due to enhanced molecular polarisation and improved binding stability.

Symmetrical substituents reduce cytotoxicity, implying an electronic imbalance that does not support strong protein interactions.

The azo group (–N=N–) plays a crucial role in biological activity by extending π-conjugation and facilitating additional π–π and hydrophobic interactions.

Author contributions

N. D.: suggesting points of research [Schemes 1], supervision, methodology development, formal analysis of all the synthesised compounds [Schemes 1], writing–review & editing. D. L.: supervision, and formal analysis of the synthesised compounds. M. M. E.: preparation of all the synthesised compounds. E. M. E. and Y. A. E. are responsible for evaluating the biological activities, conducting formal analyses, performing investigations, visualising results, and writing the original draft. A. E. A.: the molecular docking study, writing, editing and reviewing. F. A. T.: the UV-Vis study, writing, editing and reviewing, and methodology.

Conflicts of interest

The authors declare no competing interests.

Data availability

All data generated or analysed during this study are included in this published article as supplementary information (SI) files. Supplementary information is available. See DOI: https://doi.org/10.1039/d5ra07769a.

Acknowledgements

The authors are grateful and would like to thank the Academy of Scientific Research and Technology, Cairo, Egypt for their financial contribution to this research, provided through the scientist for the Next generation (SNG), (Cycle 8), grant in industry areas, Egyptian Petroleum Research Institute (EPRI), Al-Azhar University/Faculty of Science (girls), and City of Scientific Research and Technological Applications (SRTA-City). This opportunity has been pivotal in my academic and professional growth, allowing me to pursue my research with dedication and focus.

References

1 R. Rajaraman, D. L. Guernsey, M. M. Rajaraman and S. R. Rajaraman, *Cancer Cell Int.*, 2006, **6**, 1–26.
2 R. Singh, *Key Heterocyclic Cores for Smart Anticancer Drug–Design Part I*, Bentham Science Publishers, 2022.
3 J. Ceramella, D. Iacopetta, A. Catalano, F. Cirillo, R. Lappano and M. S. Sinicropi, *Antibiotics*, 2022, **11**(191), 1–23.
4 K. Shahzad Munawar, S. Muhammad Haroon, S. A. Hussain and H. Raza, *J. Basic Appl. Sci.*, 2018, **14**, 217–229.
5 C. M. da Silva, D. L. da Silva, L. V. Modolo, R. B. Alves, M. A. de Resende, C. V. B. Martins and Â. de Fátima, *J. Adv. Res.*, 2011, **2**, 1–8.
6 A. Hameed, M. Al-Rashida, M. Uroos, S. Abid Ali and K. M. Khan, *Expert Opin. Ther. Pat.*, 2017, **27**, 63–79.
7 D. Iacopetta, R. Lappano, A. Mariconda, J. Ceramella, M. S. Sinicropi, C. Saturnino, M. Talia, F. Cirillo, F. Martinelli, F. Puoci, C. Rosano, P. Longo and M. Maggiolini, *Int. J. Mol. Sci.*, 2020, **21**, 7797.
8 A. Pandurangan, N. Singh and A. K. Tiwari, *Acad. Sci.*, 2012, **4**, 5–11.
9 A. Kajal, S. Bala, S. Kamboj, N. Sharma and V. Saini, *J. Catal.*, 2013, **2013**, 1–14.

10 R. N. Sharma, F. P. Xavier, K. K. Vasu, S. C. Chaturvedi and S. S. Pancholi, *J. Enzyme Inhib. Med. Chem.*, 2009, **24**, 890–897.
11 W. D. Alrohily, M. E. Habib, S. M. El-Messery, A. Alqurshi, H. El-Subbagh and E.-S. E. Habib, *Microb. Pathog.*, 2019, **136**, 103674.
12 O. Bozdağ-Dündar, M. Ceylan-Ünlüsoy, V. Eugen and R. Ertan, *Arzneimittelforschung*, 2011, **56**, 621–625.
13 T. A. Farghaly, G. S. Masaret, Z. A. Muhammad and M. F. Harras, *Bioorg. Chem.*, 2020, **98**, 103761.
14 A. Mohammadi-Farani, A. R. Foroumadi, M. R. Kashani and A. R. Aliabadi, *Iran. J. Basic Med. Sci.*, 2014, **17**, 502–508.
15 B. Z. Kurt, I. Gazioglu, F. Sonmez and M. Kucukislamoglu, *Bioorg. Chem.*, 2015, **59**, 80–90.
16 R. K. Singh, D. N. Prasad and T. R. Bhardwaj, *Med. Chem. Res.*, 2015, **24**, 1534–1545.
17 C. Tratrat, A. Petrou, A. Geronikaki, M. Ivanov, M. Kostić, M. Soković, I. S. Vizirianakis, N. F. Theodoroula and M. Haroun, *Molecules*, 2022, **27**, 1930.
18 W. S. Liu, R. R. Wang, H. Yue, Z. H. Zheng, X. H. Lu, S. Q. Wang, W. L. Dong and R. L. Wang, *J. Biomol. Struct. Dyn.*, 2020, **38**, 3814–3824.
19 A. D. Patel, T. Y. Pasha, P. Lunagariya, U. Shah, T. Bhambharoliya and R. K. P. Tripathi, *ChemMedChem*, 2020, **15**, 1229–1242.
20 D. Kaminskyy, A. Kryshchyshyn and R. Lesyk, *Eur. J. Med. Chem.*, 2017, **140**, 542–594.
21 R. Morphy and Z. Rankovic, *J. Med. Chem.*, 2005, **48**, 6523–6543.
22 M. Bhat, B. Poojary, B. S. Kalal, P. M. Gurubasavaraja Swamy, S. Kabilan, V. Kumar, N. Shruthi, S. A. Alias Anand and V. R. Pai, *Future Med. Chem.*, 2018, **10**, 1017–1036.
23 S. D. Tupare, S. Digamber and T. K. E. S. Anandibai, *Int. J. Sci. Res.*, 2024, **9**, 292–297.
24 T. Mosmann, *J. Immunol. Methods*, 1983, **65**(1–2), 55–63.
25 E. M. El-Fakharany, W. B. Elsharkawy, Y. A. El-Maradny and H. El-Gendi, *J. Food Sci.*, 2024, **89**, 5130–5149.
26 N. T. A. Dawoud, E. M. El-Fakharany, A. E. Abdallah, H. El-Gendi and D. R. Lotfy, *Sci. Rep.*, 2022, **12**, 1–17.
27 M. A. Ebraheem, E. M. El-Fakharany, S. M. Husseiny and F. A. Mohammed, *Microb. Cell Factories*, 2024, **23**, 200.
28 S. E. El-Didamony, M. H. Kalaba, M. H. Sharaf, E. M. El-Fakharany, A. Osman, M. Sitohy and B. Sitohy, *Front. Microbiol.*, 2024, **15**, DOI: 10.3389/fmicb.2024.1419917.
29 H. M. Habib, E. M. El-Fakharany, U. D. Souka, F. M. Elsebaee, M. G. El-Ziney and W. H. Ibrahim, , DOI:DOI: 10.3390/nu14173536.
30 H. M. Habib, E. M. El-Fakharany, E. Kheadr and W. H. Ibrahim, *Sci. Rep.*, 2022, **12**, 12393.
31 A. E. Abdallah, S. I. Eissa, M. M. S. Al Ward, R. R. Mabrouk, A. B. M. Mehany and M. A. El-Zahabi, *Bioorg. Chem.*, 2021, **109**, 104695.
32 A. E. Abdallah, M. S. Alesawy, S. I. Eissa, E. M. El-Fakharany, M. H. Kalaba, M. H. Sharaf, N. M. Abo Shama, S. H. Mahmoud, A. Mostafa, A. A. Al-Karmalawy and H. Elkady, *New J. Chem.*, 2021, **45**(36), 16557–1657.
33 M. Donmez, M. Sekerci, R. Adiguzel, E. Oğuz, F. Türkan, U. Yildiko and N. Colak, *Mol. Diversity*, 2024, **29**, 1109–1127.
34 M. Islam, A. Khan, M. T. Shehzad, A. Hameed, N. Ahmed, S. A. Halim, M. Khiat, M. U. Anwar, J. Hussain, R. Csuk, Z. Shafiq and A. Al-Harrasi, *Bioorg. Chem.*, 2019, **87**, 155–162.
35 E. M. El-Fakharany, N. T. A. Dawoud, H. El-Gendi, A. E. Abdallah and D. R. Lotfy, *Egypt. J. Chem.*, 2021, **64**, 6565–6576.
36 N. T. A. Dawoud, H. El-Gendi, D. R. Lotfy, E. M. El-Fakharany and M. H. Abdellattif, *ChemistrySelect*, 2024, **9**, e202402828.
37 B. N. N. Mallappa, G. Chandra Sharma, M. Jangir, A. Sharma and N. Singh Chauhan, *Results Chem.*, 2024, **10**, 101662.
38 M. M. El-Samoly, N. T. A. Dawoud, E. M. El-Fakharany, H. M. Mashaly, D. M. Abbas and D. R. Lotfy, *Egypt. J. Chem.*, 2026, **69**, 613–622, DOI: 10.21608/ejchem.2025.415928.12225.
39 Z. Ngaini, M. A. Jefferi and S. Farooq, *Nat. Prod. Res.*, 2024, 1–10.
40 G. M. El-Sherbiny, M. H. Kalaba, A. M. Foda, A. S. E. D. Youssef, I. A. Elsehemy, E. E. Farghal and E. M. El-Fakharany, *Microb. Pathog.*, 2024, **192**, 106705.